Hydrol. Earth Syst. Sci. Discuss., 10, 11829–11860, 2013
www.hydrol-earth-syst-sci-discuss.net/10/11829/2013/
doi:10.5194/hessd-10-11829-2013

Hydrology and Earth System Sciences
Open Access
Discussions

The effect of training image and secondary data integration with multiple-point geostatistics in groundwater modeling

X. He[1], T. O. Sonnenborg[2], F. Jørgensen[2], and K. H. Jensen[1]

[1]Department of Geosciences and Natural Resource Management, Copenhagen University, Copenhagen, Denmark
[2]Geological Survey of Denmark and Greenland (GEUS), Copenhagen, Denmark

Received: 29 August 2013 – Accepted: 13 September 2013 – Published: 26 September 2013

Correspondence to: X. He (xih@geo.ku.dk)

Published by Copernicus Publications on behalf of the European Geosciences Union.

Abstract

Multiple-point geostatistic simulation (MPS) has recently become popular in stochastic hydrogeology, primarily because of its capability to derive multivariate distributions from the training image (TI). However, its application in three dimensional simulations has been constrained by the difficulty of constructing 3-D TI. The object-based TiGenerator may be a useful tool in this regard; yet the sensitivity of model predictions to the training image has not been documented. Another issue in MPS is the integration of multiple geophysical data. The best way to retrieve and incorporate information from high resolution geophysical data is still under discussion. This work shows that TI from TiGenerator delivers acceptable results when used for groundwater modeling, although the TI directly converted from high resolution geophysical data leads to better simulation. The model results also indicate that soft conditioning in MPS is a convenient and efficient way of integrating secondary data such as 3-D airborne electromagnetic data, but over conditioning has to be avoided.

1 Introduction

Aquifer heterogeneity is one of the severe challenges in groundwater flow simulation and with limited observations it is always difficult to depict the complete subsurface geology. Hence, statistical methods are often used to estimate geological heterogeneity. Various geostatistical methods have been developed, including variogram-based techniques (Delhomme, 1979; Deutsch and Journel, 1992; Wingle and Poeter, 1993; Johnson, 1995; Klise et al., 2009), the transition probability-based method (Carle and Fogg, 1996), object-based modeling (Deutsch and Wang, 1996) and the multiple-point geostatistical approach (MPS) (Journel, 1993; Guardiano and Srivastava, 1993; Strebelle, 2002). Most of these methods require observations for interpolation, and some even have the ability to integrate multiple sources of observations. With the development in geophysical technology, high resolution geophysical mapping techniques are

HESSD
10, 11829–11860, 2013

now available, such as the airborne electromagnetic system, SkyTEM (Sørensen and Auken, 2004), ground penetrating radar (GPR) (Clement and Ward, 2008), and satellite remote sensing (Hoffmann, 2005). Bourges et al. (2012) illustrate different ways of applying gravity data, refraction seismic data and borehole data with geostatistical methods. However, the proper method to incorporate these data into geostatistical simulation is still a subject of active research.

The theory of multiple-point geostatistics has been developed over the last two decades. An important development was the pixel-based single normal equation simulation algorithm (SNESIM) proposed by Strebelle (2002), which allowed for simulations with reasonable computational power. The primary advantage of MPS is its capability to capture multiple-point based structure information instead of using 2-point based statistics (variogram) (Journel, 2005). The database from which the structural information is retrieved is referred to as a training image (TI). Comunian et al. (2011) pointed out that a 3-D TI is necessary for 3-D MPS simulation, but it is not trivial to generate a 3-D TI since geological observations generally only provide 2-D information. Hence, 3-D applications are one of the most important challenges for MPS (Huysmans and Dassargures, 2009). While a few attempts on producing 3-D TI have been presented in different but complicated ways (Coz et al., 2011; Comunian et al., 2011), Maharaja (2008) proposed a simple object based algorithm, TiGenerator, to generate parametric images. However, an image purely generated by stochastic methods lacks evidence from geological observations, and its application in MPS can be questioned. Huysmans and Dassargures (2009) concluded that the sensitivity of the model predictions to the training image is an interesting topic for further research.

Another advantage of MPS is the ability to incorporate multiple sources of data (Liu et al., 2005; Strebelle, 2006; Hu and Chugunova, 2008). With the flourish of new measurement technics, geological observations with relatively high resolution and accuracy are available, and integrating them into stochastic simulations is appealing. Liu et al. (2004) demonstrated how integration of seismic data reduces the uncertainty in geofacies simulation, other researches (Strebelle et al., 2002; Huysmans and

HESSD
10, 11829–11860, 2013

Dassargues, 2012) also applied soft data conditioning in MPS, but the specific effect of soft data conditioning on the groundwater flow regime has rarely been studied.

In this study, four scenarios of stochastic realizations were generated, with the purpose of evaluating the sensitivity of training images in MPS, as well as exploring the effect of integrating soft data in MPS simulations. The equifinality of stochastic realizations were then analysed through the steady state groundwater model simulations of hydraulic head, particle travel time and capture zone.

2 Study area and data

The study area covers a 14.5 km by 13.9 km region which is located near Ølgod in western Denmark (Fig. 1). This area is dominated by arable land with inland marsh around seven streams. The land surface elevation in this area reach values of about 64 m above mean sea level (a.s.l.) in the north western part, and decreases to around 17 m a.s.l. in the south eastern part. The climate in this area is characterized by mean temperatures ranging from 1.4 °C in January to 16.5 °C in August with annual average around 8.2 °C. Precipitation is concentrated in autumn and winter while spring is relatively dry, the average annual precipitation is approximately 1050 mm yr^{-1} (Stisen et al., 2011). Water consumption primarily relies on groundwater abstraction. According to the National Water Resources Model (Henriksen et al., 2003), the annual average groundwater recharge is 611 mm yr^{-1}. According to the Danish national geological database JUPITER (http://www.geus.dk/jupiter/index-dk.htm), there are 165 pumping wells in this area with total mean abstraction of 3.2×10^6 m^3 yr^{-1} in the period 2000 to 2010.

Intensive geological surveys show that this area is dominated by highly heterogeneous Quaternary sediments with variable thickness above −100 m a.s.l. (Høyer et al., 2011). Below Miocene deposits are located with a thickness of up to about 150 m and with Paleogene clay at the bottom (Rasmussen et al., 2010). The JUPITER database holds geological descriptions from 525 boreholes in the study area, but only

HESSD
10, 11829–11860, 2013

22 boreholes reach deeper than −70 m a.s.l. Therefore, the geological analysis and modeling were performed for Quaternary sediments from the surface to −70 m a.s.l. The geological settings have been conceptualized into five units: Quaternary sand, Quaternary clay, Miocene sand, Miocene clay and Paleogene clay. The borehole description was therefore also categorized accordingly.

Another important source of information is the airborne transient electromagnetic (SkyTEM) data (Høyer et al., 2011). The subsurface electrical resistivity data were collected with line spacing from 125 m to 270 m, and the soundings penetrated down to more than 200 m. The data have been discretized and interpolated into a 3-D grid with cell size of 100 m × 100 m × 5 m. With its high resolution, SkyTEM data are ideal as soft probability data or training image for MPS simulation.

Besides the geological data, a detailed geological model has also been developed for the area (Jørgensen et al., 2012). The model was developed using non-linear inversion to estimate the clay content from SkyTEM resistivity and borehole data (SSV model) (Foged and Christiansen, 2013). The SSV model categorized Quaternary sediment into ten classes regarding clay content. In this study the model was simplified into a binary sand-clay model by assigning classes with clay content up to 60 % as Quaternary sand, and the rest as Quaternary clay.

3 Methodology

3.1 Multiple-point geostatistics

Multiple-point geostatistics (MPS) was first presented as a direct algorithm in stochastic simulation by Guardiano and Srivastava (1993), and Strebelle (2002) introduced the single normal equation sequential simulation (SNESIM) algorithm which combines the flexibility of the pixel-based algorithm and the ability to reproduce crisp shapes of the object-based algorithm. The critical step of sequential simulation is the conditional probability distribution function (cpdf), and in the SNESIM algorithm it is solved by the

HESSD
10, 11829–11860, 2013

following equation:

$$P\left(U;S_k|(n)\right) = \text{Prob}\left\{S(U) = S_k|S(U_a) = S_{ka}\right\} \cong \frac{c_k(d_n)}{c(d_n)} \quad (1)$$

This solution is achieved by scanning a training image. A training image (TI) is a conceptual 2-D or 3-D map which depicts the expected structure and pattern of facies (Strebelle, 2002). TI is scanned by a template consisting of $n+1$ nodes and is centered at location U, the values $c(d_n)$ and $c_k(d_n)$ are recorded while scanning TI. d_n denotes the data event of all n surrounding nodes. $c(d_n)$ denotes the number of replicates of the conditioning data event $d_n = \{S(U_a) = S_{ka}, a = 1,\cdots,n\}$, and $c_k(d_n)$ denotes that among those $c(d_n)$ replicates, the number of replicates with the central node U has the value $S(U) = S_k$. Therefore, Eq. (1) implies that the probability of state S_k to occur at location U with n neighbor data is equal to the training proportion $c_k(d_n)/c(d_n)$.

With the possession of cpdf, the sequential simulation paradigm by Goovaerts (1997, p. 376) is used in stochastic simulation. The hard data is first assigned to the closest grid nodes, and all the unknown grids are visited once and only once in a random path. At each unknown location U, the recorded cpdf corresponding to actually presented hard conditioning data event are retrieved, and is used to draw the simulated value S at this location.

3.2 Soft data conditioning

Soft data or secondary data indicate data that provide indirect information on the distribution of geological facies. Typical soft data include geophysical data such as seismic data, space borne geodetic observations, and airborne electromagnetic data. To be integrated in SNESIM, soft data first have to be converted into facies probability data (Strebelle, 2006).

Let n be the facies indicator value at location U, then $P(A)$ is the facies global proportion or prior probability in Bayesian statistical term. B infers to data event from training image, and then the notation $P\left(U;S_k|(n)\right)$ in Eq. (1) can be rewritten as $P\left(A|B\right)$. Let

HESSD
10, 11829–11860, 2013

C represents the additional soft information, and then $P(A|C)$ denotes the probability derived from soft data. Journel (2002) derived a Bayesian based model of integrating $P(A|B)$ and $P(A|C)$:

$$P(A|B,C) = \frac{a^{\tau}}{a^{\tau} + b \cdot c^{\tau}} \in [0,1] \tag{2}$$

where

$$a = \frac{1 - P(A)}{P(A)} \tag{3}$$

$$b = \frac{1 - P(A|B)}{P(A|B)} \tag{4}$$

$$c = \frac{1 - P(A|C)}{P(A|C)} \tag{5}$$

The parameter τ is used to adjust the contribution of soft information C. $\tau = 1$ indicates independence of contribution of data C from data B. For $\tau = 0$ the soft information is ignored, while for $\tau > 1$ the influence of soft data C is increased, and it is decreased for $\tau < 1$.

3.3 SkyTEM data to soft probability

In this study we applied a supervised technique (Liu et al., 2005) to retrieve probabilistic information from SkyTEM data. The SkyTEM data was converted to facies probability data by correlating the facies occurrence in boreholes with SkyTEM resistivity. For every 0.2 m borehole log, the sediment was categorized as sand or clay and the corresponding SkyTEM resistivity value was recorded. Subsequently for each resistivity bin (size 1 Ω m) the sand probability based on borehole data was computed and plotted against corresponding SkyTEM resistivity (Fig. 2). The data points were

HESSD
10, 11829–11860, 2013

fitted by a non-linear regression function (green line), which was used to convert the 3-D SkyTEM data into a 3-D sand probability map. Due to data noise, curve fitting was performed for resistivity between 10 and 140 Ω m (Eq. 6). The coefficient of determination is 0.80 and the Root Mean Square Error (RMSE) is 0.08. For resistivity lower than 10 Ω m there are only two data points both with sand occurrence at 0, and thus sand occurrence was set to 0 below this value. For resistivity higher than 140 Ω m, 80 % data points show sand occurrence at 1, thus the corresponding sand occurrence was set to 1. The membership function is therefore expressed as

$$P_s = \begin{cases} 1 & \text{if } R > 140\ \Omega\,\text{m} \\ 0.0863 \times (\ln R)^3 - 0.958 \times (\ln R)^2 & \\ +3.759 \times (\ln R) - 4.596 & \text{if } 10\ \Omega\,\text{m} \ll R \ll 140\ \Omega\,\text{m} \\ 0 & \text{if } R < 10\ \Omega\,\text{m} \end{cases} \quad (6)$$

where R is the SkyTEM resistivity. Figure 3 shows Quaternary sand probability distributions as derived from Eq. (6) for lateral and vertical cross-sections.

3.4 Training image

Construction of 3-D TI is challenging since most geostatistical descriptive maps are only in 1-D or 2-D. In this study two kinds of 3-D training images were generated, denoted TI1 and TI2 respectively.

TI1 was directly converted from SkyTEM data. Based on the resistivity the subsurface was divided into Quaternary sand and Quaternary clay by using a critical resistivity value. According to the 525 borehole logs, the proportion of Quaternary clay is 0.33. This proportion is assumed to be representative of the study area, although it could be slightly biased due to the uneven distribution of borehole. Figure 4 shows the cumulative probability distribution curve of resistivity data. The Quaternary clay proportion 0.33 corresponds to 41.6 Ω m on the SkyTEM resistivity cpdf curve. Thus, for resistivity below this value the sediment is categorized as Quaternary clay, while for resistivity

HESSD
10, 11829–11860, 2013

above the sediment is categorized as Quaternary sand. Figure 5 (left) illustrates cross sections of TI1.

TI2 was generated by the TiGenerator (Maharaja, 2008), which is part of SGeMS's (Stanford Geostatistical Modeling Software) package. The TiGenerator (Maharaja, 2008) provides a method for generating 3-D training images with parametric shapes using non-iterative, unconditional Boolean simulation. The user-defined geometry and orientation of simulated objects can be deterministic or statistical described. With the current version geobodies with shapes of sinusoid, ellipsoid, half-ellipsoid and cuboid can be defined with given geometric parameters such as maximum radius, median radius, and minimum. The geobody is drawn by following a random path until the facies proportion is fulfilled in the simulated grid.

Parameters of proportion and geometry of Quaternary clay bodies were obtained by interpretation of TI1. Quaternary sand was taken as background facies with a proportion of 0.67, in which the Quaternary clay bodies were embedded. The size of Quaternary clay bodies in TI1 was scanned in X, Y, Z direction separately, and the distribution of size in each direction was computed (Table 1). These properties were adopted for the geometry of ellipsoid clay bodies in the TiGenerator. Figure 5 (right) shows the cross sections of TI2. Compared to TI1 on the left, the shapes of clay bodies in TI2 are more homogeneous and in the form of ellipsoids of various sizes, while in TI1 the size and shape of clay bodies are more heterogeneous.

3.5 Groundwater model

The groundwater modeling code MODFLOW-2000 (Harbaugh et al., 2000) was used to assess the effect of geological model on the groundwater flow regime, explicitly on simulated hydraulic head. In addition the particle tracking post-processing code MODPATH (Pollock, 1994) was used to simulate groundwater travel time and capture zone.

The groundwater model extends down to −300 m a.s.l. However, as stated previously, due to the sparse data at depth, stochastic geological modeling was only applied

HESSD
10, 11829–11860, 2013

from soil surface to −70 m a.s.l. Below, the comparably more homogeneous Miocene sediment starts to dominate, and the structure from the SSV model was applied. In order to resemble the finely discretized geological model (100 m × 100 m × 5 m), the Hydrogeologic-Unit Flow (HUF) package (Evan and Mary, 2000) was used. The groundwater model was discretized to 63 layers with cells of 100 m × 100 m horizontally, resulting in a total of 792 603 active cells. A constant layer thickness of 5 m is used from layer 6 to 63, and to avoid dry cells the top layer is 13 m thick on average, while the thickness of layer 2 to 5 is 4 m on average.

3.6 Ensemble analysis

To test the effect of training image and soft conditioning on geostatistical realizations, multiple-point geostatistical simulations were carried out by applying four different combinations of TI and soft conditioning, see Table 2. According to He et al. (2013) the variation of simulated hydraulic head tends to be stable after accumulating 30 model runs. Hence, in this study 50 realizations were generated for each scenario and subsequently anchored to the steady state groundwater model. In total 200 MODFLOW models were developed. The simulated groundwater head, groundwater travel time and capture zones were evaluated by comparison to a reference model – the SSV model, whose geology was modelled independently. Similar to the four scenarios, the SSV model is also a 3-D binary sand-clay model. SSV is developed as an independent method which by inversion optimizes the relation between resistivity and borehole data in each grid cell in combination with the geologist's expert knowledge (Foged and Christiansen, 2013; Jørgensen et al., 2012). The SSV model is assumed to give the most accurate description of the study area.

All groundwater models share the same values of the hydraulic parameters for the respective geological units. As field information on hydraulic conductivity is sparse, the inversion code PEST (Doherty, 2005) was used to estimate the hydraulic conductivity of Quaternary sand, Quaternary clay and Miocene sand. The geological model SSV was applied for estimation, which resulted in the following parameter estimates: 4.8 m d^{-1}

HESSD
10, 11829–11860, 2013

for Quaternary sand, $0.7 \times 10^{-3}\,m\,d^{-1}$ for Quaternary clay and $3.9\,m\,d^{-1}$ for Miocene sand. Hydraulic conductivities of $0.5 \times 10^{-3}\,m\,d^{-1}$ and $8.6 \times 10^{-4}\,m\,d^{-1}$ were assigned to Miocene clay and Paleogene clay.

4 Result and discussion

Based on the flow solutions backward particle tracking and capture zone were carried out for each model by using MODPATH. All model simulations were compared to the reference model, namely the model with SSV geological structure.

4.1 Groundwater head

There are 137 observation wells which are screened above level −70 m a.s.l. in the model area (Fig. 1). RMSE for the 137 wells was calculated based on simulation results of each realization of geology and the simulation of the SSV model. Based on the 50 realizations the mean, μ_{RMSE}, and standard deviation, σ_{RMSE}, of RMSE of each scenario are listed in Table 3. Comparison of simulations with and without soft data shows that results from simulations without soft data (S1 and S3) have the largest RMSE values, while the mean of RMSE for S2 and S4 have similar and smaller values than those from S1 and S3. This indicates that the accuracy of the simulations is improved when applying soft conditioning for both training images. However, application of soft data also affects the variability between the flow solutions as expressed by the standard deviation of the RMSE values. A standard deviation of 0.7 m is found for both S2 and S4 while the standard deviation for the realizations not using soft data is considerable higher (1.0 m and 1.2 m).

The impact of training image is seen by comparing S1 and S2 using TI1 to S3 and S4 using the TiGenerator based TI2. The results show that realizations with TI1 have higher accuracy in groundwater head simulation than those generated with TI2. However, the difference in mean RMSE between realizations generated with TI1 and TI2 is

HESSD
10, 11829–11860, 2013

less than the difference found using realization with and without soft data. Therefore, even though TI2 is a relatively poor representation of the geological structure, the simulation yields acceptable results. With respect to variability between the realizations, represented by σ_{RMSE}, the choice of training image has a relatively small effect.

Figure 6 illustrates the standard deviation of simulated hydraulic head from each scenario. The overall hydraulic head distribution is affected by the pattern of training image. Models using TI1 (S1 and S2) show more discrete patterns than the ones using TI2 (S3 and S4). This is probably because TI2 is composed of the more homogeneous ellipsoid clay bodies, while TI1 is composed of clay bodies with a highly discrete and heterogeneous pattern (Fig. 5). Furthermore, by comparing the simulations with soft conditioning (S2 and S4) with the ones without soft conditioning (S1 and S3), it is obvious that the overall standard deviation is decreased when conditioning with soft data. Another interesting phenomenon is that the reduction in uncertainty from S1 to S2 is higher than that from S3 to S4.

This phenomenon is also illustrated in Fig. 7, in which the E-type map (cell-wise arithmetic average) of 50 realizations from each scenario is compared against soft data with Q-Q plot. The *x* axis shows the clay probability from soft data, while the *y* axis shows the corresponding probability from the E-type map. Therefore, the Q-Q plot can be evaluated against the probability distribution of clay probability from soft data, represented by the black line in the figure. The closer the Q-Q plot is to the black line, the more information is derived from the soft data. While the plot for S1 is far from the black line, the plot for S2 (blue plot) is much closer. The red plot (S4) is also closer to the black line than the purple plot (S3). However, the difference between S1 (yellow plot) and S2 (blue plot) is larger than that of S3 (purple plot) and S4 (red plot), and this is coherent with the differences in hydraulic head uncertainties presented in Fig. 6. The reason for this is the data dependency. Both TI1 and soft data are derived from the SkyTEM data, and although they were processed in different ways, they are not totally independent. In Eq. (2), the parameter τ is used to adjust the dependence between two data sets. To make S2 and S4 comparable, we set parameter τ to 1.0 in

HESSD
10, 11829–11860, 2013

both cases. Liu (2006) also pointed out that using a value of 1.0 generates the most robust results. In Fig. 7 the plot for S2 (blue) is lower than the black line in the low probability part, while it is located above the black line in the high probability part, indicating that the S2 realizations are over conditioned. In contrast, as TI2 is remotely related with the soft data, the soft conditioning on S4 improves the simulations but do not result in over condition. Therefore, the integration of TI2 with soft data is sounder than the combination of TI1 and soft data. Journel (2002) mentioned that when $\tau < 1$ the influence from additional data is decreased. Therefore, another scenario (S5) was added where TI1 and soft data were used, but the parameter τ is set to 0.5. S5 corresponds to the green plot in Fig. 7, and it is located right between S1 and S2, which illustrates the effect of decreasing τ.

4.2 Particle tracking and capture zone

Backward particle tracking was also simulated for the 137 points. The particle travel times simulated by SSV model were taken as the reference values and for each scenario RMSE was computed by relating to the reference (Table 4). Similar to the results for hydraulic head, the mean RMSE from S1 and S3 is comparable, which indicates that even though TI2 only contains randomly distributed ellipsoid clay bodies, the simulation for groundwater age is not particularly worse than when simulated with TI1. Also similar to hydraulic head simulations, the mean of RMSE from S2 is smaller than that of S1, and same applies to S4 and S3. This indicates that soft conditioning helped to constrain the heterogeneity.

Probabilistic capture zones were analysed for three abstraction wells screened in both shallow and deep layers. Figure 8 to 10 show the probabilistic capture zone for these three wells. In each figure the top row illustrates the capture zones for S1 and S2, while the second row represents the corresponding simulations from S3 and S4. Generally, there are no distinct differences between first and second row, which again implies that realizations from TI2 appear acceptable. For all three wells, the simulation for S2 has smaller area and more concentrated high probability area than the one

HESSD
10, 11829–11860, 2013

from S1, again suggesting that for simulations with TI1, the soft data constrain the geological heterogeneity. However, such tendency is not seen for simulations with TI2. The sizes of the capture zones are similar for simulation S3 and S4 for Well 1 and Well 2 respectively, and for Well 3 in layer 15 (Fig. 11), the one with soft conditioning (S4) is even larger than the one without (S3). The explanation for this is again data redundancy as for hydraulic head. Realizations from S2 have been over conditioned and therefore the uncertainty on probabilistic capture zone has been constrained extremely.

5 Conclusions

This study is one of the first to evaluate the behaviour of geophysical data in multiple-point geostatistics simulation. It demonstrates how the 3-D high resolution airborne electromagnetic data can be used as training image (TI) as well as secondary data for soft conditioning. The sensitivity of model predictions to TI and soft conditioning has also been analysed. The SkyTEM derived training image which resembles the actual geological structure at the site was evaluated against the parametric training image generated by the object-based TiGenerator. TI from TiGenerator is an abstract depiction of geological structure with parameterized geometry. Although it holds less accuracy in heterogeneity in comparison to the TI derived from field data, it was found to be a reasonable input to MPS. Comparison for groundwater heads indicated that a training image with higher accuracy helped improving the model simulation. Nevertheless, TI from TiGenerator proved to be an acceptable option in MPS, as a TI with less precise representation of the field structure did not significantly degrade the simulation.

By further conditioning on secondary data, the groundwater head simulation was improved both with respect to higher accuracy and lower uncertainty, which underlines the advantages of the MPS method. However, when applying soft conditioning, the dependence of different data sets has to be taken into account. If the training image and the soft conditioning data are based on the same source of information, the resulting geological realizations may be over-conditioned resulting in under prediction of the

HESSD
10, 11829–11860, 2013

uncertainties of flow and transport simulations. This was demonstrated for the examined case where high-resolution SkyTEM data was used as both training image and soft conditioning which resulted in a higher reduction in capture zone uncertainty than if SkyTEM was only used for soft conditioning. Therefore, it is recommended to use independent data sources for generating the training image and the soft data, e.g., by utilizing geophysical data for soft conditioning while using the TiGenerator for defining the training image. The information required by the TiGenerator may be derived from expert knowledge on the geological structure at the site or derived from analysis of the mapped geology at a site with comparable geology. Alternatively, a Q-Q plot analysis could be carried out and the contribution from soft data on the realization should be decreased. It is however Eq. (1) problematic to estimate the optimal level of information which should be contained from the soft data and Eq. (2) time consuming to carry out the analysis.

References

Bourges, M., Mari, J.-L., and Jeannée, N.: A practical review of geostatistical processing applied to geophysical data: methods and applications, Geophys. Prospect., 60, 400–412, 2012.

Carle, S. F. and Fogg, G. E.: Transition probability-based indicator geostatistics, Math. Geol., 28, 453–476, 1996.

Clement, W. P. and Ward, A.: GPR surveys across a prototype surface barrier to determine temporal and spatial variations in soil moisture content, chapter 23, in: The Handbook of Agricultural Geophysics, edited by: Allred, B. J., Ehsani, M. R., and Daniels, J. J., American Society of Agricultural Engineers, CRC Press, 305–315, 2008.

Comunian, A., Renard, P., Straubhaar, J., and Bayer, P.: Three-dimensional high resolution fluvio-glacial aquifer analog – Part 2: geostatistical modeling, J. Hydrol., 405, 10–23, 2011.

Coz, M. L., Genthon, P., and Adler, P. M.: Multiple-point statistics for modeling facies heterogeneities in a porous medium: the Komadugu-Yobe Alluvium, Lake Chad Basin, Math. Geosci., 43, 861–878, 2011.

Delhomme, J. P.: Spatial variability and uncertainty in groundwater flow parameters: a geostatistical approach, Water Resour. Res., 15, 269–280, 1979.

HESSD
10, 11829–11860, 2013

Doherty, J.: PEST: Model Independent Parameter Estimation, 5th edn. of user manual, Watermark Numerical Computing, Brisbane, Australia, 2005.
Deutsch, C. V. and Journel, A. G.: GSLIB Geostatistical Software Library and User's Guide, Oxford University Press, New York, 1992.
Deutsch, C. V. and Wang, L.: Hierarchical object-based stochastic modeling of fluvial reservoirs, Math. Geol., 28, 857–880, 1996.
Evan, R. A. and Mary, C. H.: Documentation of the hydrogeologic-unit flow (HUF) package, US Geological Survey Open File Rep 00-342, US Geological Survey, Denver, CO, USA, 2000.
Foged, N. and Christiansen, A. V.: Large-Scale Automatic Generation of Lithological Models from Resistivities Using Borehole Information in an Inversion Approach, SAGEEP, Denver, Colorado, 2013.
Goovaerts, P.: Geostatistics for Natural Resources Evaluation, Oxford University Press, New York, 483 pp., 1997.
Guardiano, F. B. and Srivastava, R. M.: Multivariate Geostatistics: Beyond Bivariate Moments, in: Geostatistics Tróia '92, Quantitative Geology and Geostatistics, edited by: Soares, A., Kluwer Academic Publishers, Dordrecht, Netherlands, 133–144, 1993
Harbaugh, A. W., Banta, E. R., Hill, M. C., and McDonald, M. G.: MODFLOW-2000, the US Geological Survey modular ground-water model – user guide to modularization concepts and the Ground-Water Flow Process: US Geological Survey Open-File Report 00-92, US Department of Interior, Reston, VA, USA, 121 pp., 2000.
He, X., Sonnenborg, T. O., Jørgensen, F., Høyer, A.-S., Møller, R. R., and Jensen, K. H.: Analyzing the effects of geological and parameter uncertainty on prediction of groundwater head and travel time, Hydrol. Earth Syst. Sci., 17, 3245–3260, doi:10.5194/hess-17-3245-2013, 2013.
Henriksen, H. J., Troldborg, L., Nyegaard, P., Sonnenborg, T. O., Refsgaard, J. C., and Madsen, B.: Methodology for construction, calibration and validation of a national hydrological model for Denmark, J. Hydrol., 280, 52–71, 2003.
Hoffmann, J.: The future of satellite remote sensing in hydrogeology, Hydrogeol. J., 13, 247–250, 2005.
Hu, L. Y. and Chugunova, T.: Multiple-point geostatistics for modeling subsurface heterogeneity: a comprehensive review, Water Resour. Res., 44, W11413, doi:10.1029/2008WR006993, 2008.

HESSD
10, 11829–11860, 2013

Huysmans, M. and Dassargues, A.: Application of multiple-point geostatistics on modelling groundwater flow and transport in a cross-bedded aquifer (Belgium), Hydrogeol. J., 17, 1901–1911, 2009.
Huysmans, M. and Dassargues, A.: Modeling the effect of clay drapes on pumping test response in a cross-bedded aquifer using multiple-point geostatistics, J. Hydrol., 450–451, 159–167, 2012.
Høyer, A.-S., Lykke-Andersen, H., Jørgensen, F., and Auken, E.: Combined interpretation of SkyTEM and high-resolution seismic data, Phys. Chem. Earth A/B/C, 36, 1386–1397, 2011.
Johnson, N. M.: Characterization of alluvial hydrostratigraphy with indicator semivariograms, Water Resour. Res., 31, 3217–3227, 1995.
Journel, A. G.: Geostatistics: roadblocks and challenges, in:, Geostatistics Tróia '92, edited by: Soares, A., Springer Netherlands, Dordrecht, 213–224, 1993.
Journel, A. G.: Combining knowledge from diverse sources: an alternative to traditional data independence hypotheses, Math. Geol., 34, 573–596, 2002.
Journel, A. G.: Beyond covariance: the advent of multiple-point geostatistics, in: Geostatistics Banff 2004, Quantitative Geology and Geostatistics, edited by: Leuangthong, O. and Deutsch, C. V., Springer Netherlands, Dordrecht, Netherlands, 225–233, 2005.
Jørgensen, F., Møller, R. R., Høyer, A. H., and Christiansen, A. V.: Geologisk model ved Ølgod og Skovlund – eksempel på effektiviseret modellering i et heterogent geologisk miljø, Danmarks og Grønlands Geologiske Undersøgelse Rapport 2012/82, 83 pp., 2012.
Klise, K. A., Weissmann, G. S., McKenna, S. A., Nichols, E. M., Frechette, J. D., Wawrzyniec, T. F., and Tidwell, V. C.: Exploring solute transport and streamline connectivity using lidar-based outcrop images and geostatistical representations of heterogeneity, Water Resour. Res., 45, W05413, doi:10.1029/2008WR007500, 2009.
Liu, Y.: Using the Snesim program for multiple-point statistical simulation, Comput. Geosci., 32, 1544–1563, 2006.
Liu, Y., Harding, A., Abriel, W., and Strebelle, S.: Multiple-point simulation integrating wells, three-dimensional seismic data, and geology, AAPG Bull., 88, 905–921, 2004.
Liu, Y., Harding, A., Gilbert, R., and Journel, A. G.: A workflow for multiple-point geostatistical simulation, in: Geostatistics Banff 2004, Quantitative Geology and Geostatistics, edited by: Leuangthong, O. and Deutsch, C. V., Springer Netherlands, Dordrecht, Netherlands, 245–254, 2005.

HESSD
10, 11829–11860, 2013

Maharaja, A.: TiGenerator: object-based training image generator, Comput. Geosci., 34, 1753–1761, 2008.
Pollock, D. W.: User's guide for MODPATH/MODPATH-PLOT a particle tracking post-processing package for MODFLOW, the US Geological Survey finite-difference ground-water flow model (SuDoc I 19.76:94-464). The Survey Earth Science Information Center, Open-File Reports Section, distributor, 1994.
Rasmussen, E. S., Dybkjær, K., and Piasecki, S.: Lithostratigraphy of the Upper Oligocene – Miocene succession of Denmark, Geological Survey of Denmark and Greenland Bulletin, Geological Survey of Denmark, Copenhagen, Denmark, 22, 92 pp., 2010.
Stisen, S., Sonnenborg, T. O., Højberg, A. L., Troldborg, L., and Refsgaard, J. C.: Evaluation of climate input biases and water balance issues using a coupled surface–subsurface model, Vadose Zone J., 10, 37–53, 2011.
Strebelle, S.: Conditional simulation of complex geological structures using multiple-point statistics, Math. Geol., 34, 1–21, 2002.
Strebelle, S. B.: Sequential simulation for modeling geological structures from training images, in: Stochastic Modeling and Geostatistics: Principles, Methods, and Case Studies, Volume II: AAPG Computer Applications in Geology 5, edited by: Coburn, T. C., Yarus, J. M., and Chambers, R. L., AAPG, Tulsa, OK, USA, 139–149, 2006.
Strebelle, S. B., Payrazyan, K., and Caers, J.: Modeling of a deepwater turbidite reservoir conditional to seismic data using multiple point geostatistics. Society of Petroleum Engineers (SPE) Annual Conference and Technical Meeting, SPE 77429, San Antonio, TX, 2002.
Sørensen, K. I. and Auken, E.: SkyTEM – a new high-resolution helicopter transient electromagnetic system, Explor. Geophys., 35, 191–199, 2004.
Wingle, W. L. and Poeter, E. P.: Uncertainty associated with semivariograms used for site simulation, Ground Water, 31, 725–734, 1993.

HESSD
10, 11829–11860, 2013

Table 1. The size distribution of Quaternary clay bodies. Unit: m.

	Minimum	Median	Maximum
X	50	250	2950
Y	50	250	3200
Z	2.5	20	60

HESSD
10, 11829–11860, 2013

Table 2. Four scenarios of geological realizations used for multiple-point geostatistic simulation.

Scenario	Training Image	Soft Condition
S1	TI1	No
S2	TI1	Yes
S3	TI2	No
S4	TI2	Yes

HESSD
10, 11829–11860, 2013

Table 3. RMSE of simulated hydraulic head against SSV simulation. The table lists mean, μ_{RMSE}, and standard deviation, σ_{RMSE}, over 50 realizations (where each RMSE value is based on 137 observation wells).

	μ_{RMSE} (m)	σ_{RMSE} (m)
S1	1.4	1.0
S2	0.8	0.7
S3	1.7	1.2
S4	1.0	0.7

HESSD
10, 11829–11860, 2013

Table 4. RMSE of simulated particle travel time against SSV simulation. The table lists mean, μ_{RMSE}, and standard deviation, σ_{RMSE}, over 50 realizations (where each RMSE values are based on backward particle tracking for 137 cells).

	μ_{RMSE} (yr)	σ_{RMSE} (yr)
S1	45	149
S2	40	126
S3	39	139
S4	36	128

HESSD
10, 11829–11860, 2013

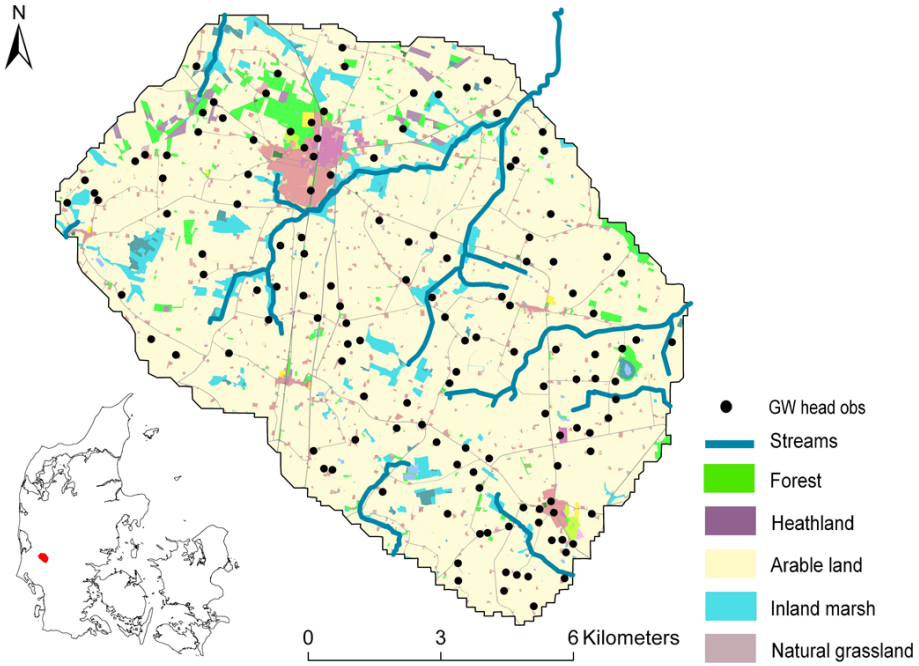

Fig. 1. Location and land use of study area. Black points denote 137 boreholes for groundwater head observation.

HESSD
10, 11829–11860, 2013

The effect of TI and data integration with MPS in groundwater modeling

X. He et al.

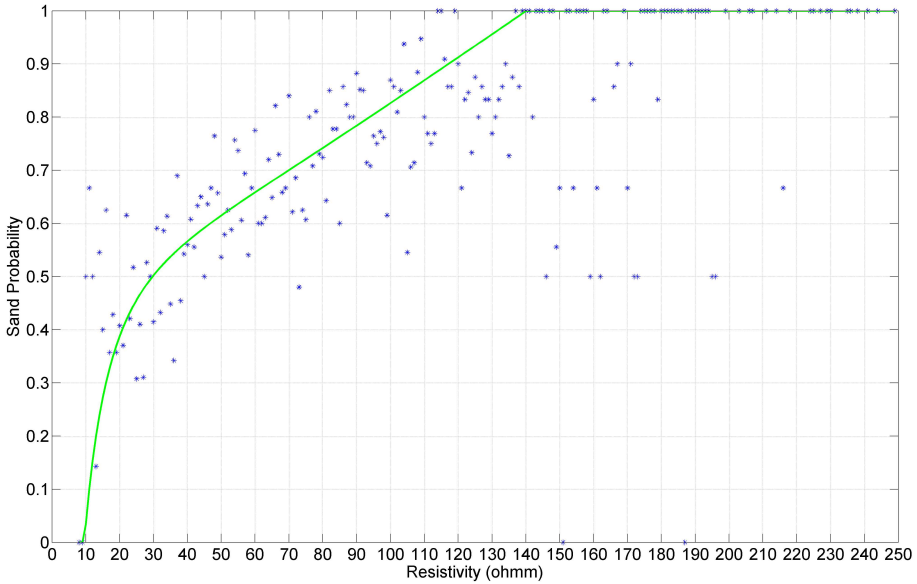

Fig. 2. Non-linear regression of sand occurrence against SkyTEM resistivity. Blue points are sand occurrence from borehole data pared to SkyTEM resistivity. Green line is the regression line (Eq. 6), coefficient of determination is 0.80 and RMSE is 0.08.

HESSD
10, 11829–11860, 2013

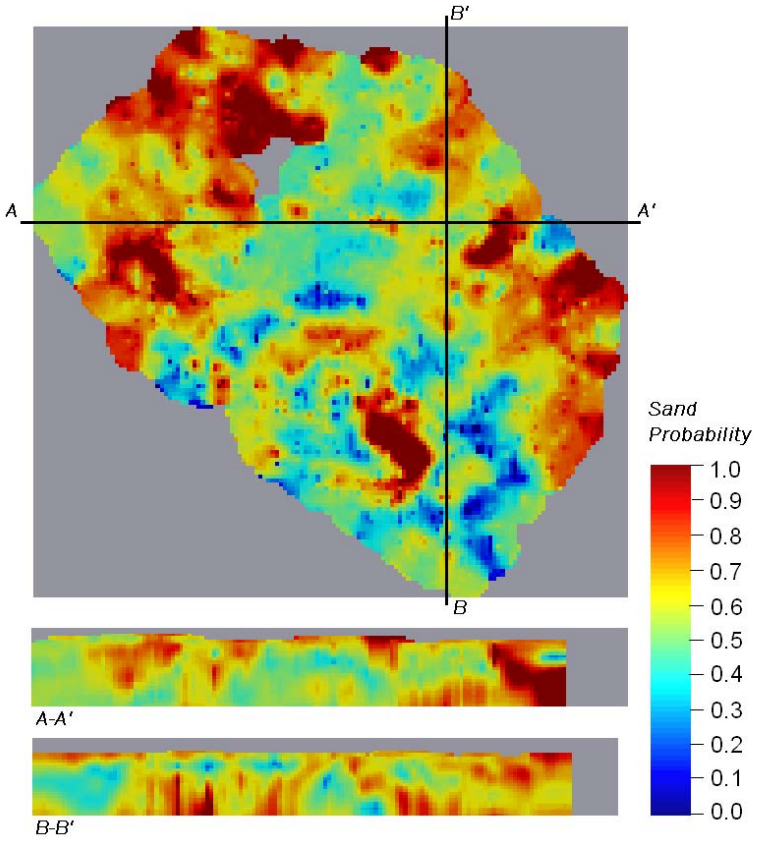

Fig. 3. Cross sections of 3-D map showing probability of Quaternary sand. Lateral cross section is taken at 10 m a.s.l., vertical exaggeration is 15.

HESSD
10, 11829–11860, 2013

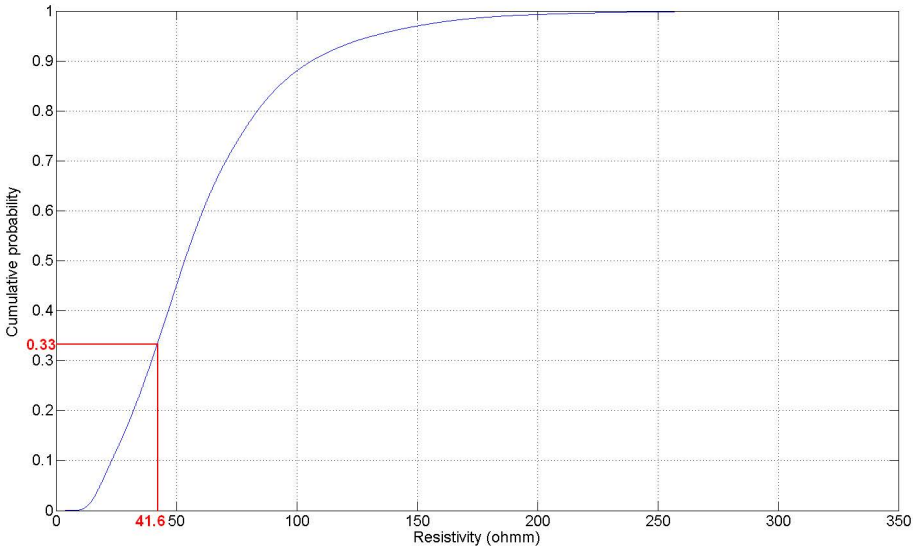

Fig. 4. Cumulative probability distribution curve of SkyTEM resistivity. Resistivity of 41.6 Ω m corresponds to a proportion of 0.33, which is the proportion of Quaternary clay according to borehole data.

HESSD
10, 11829–11860, 2013

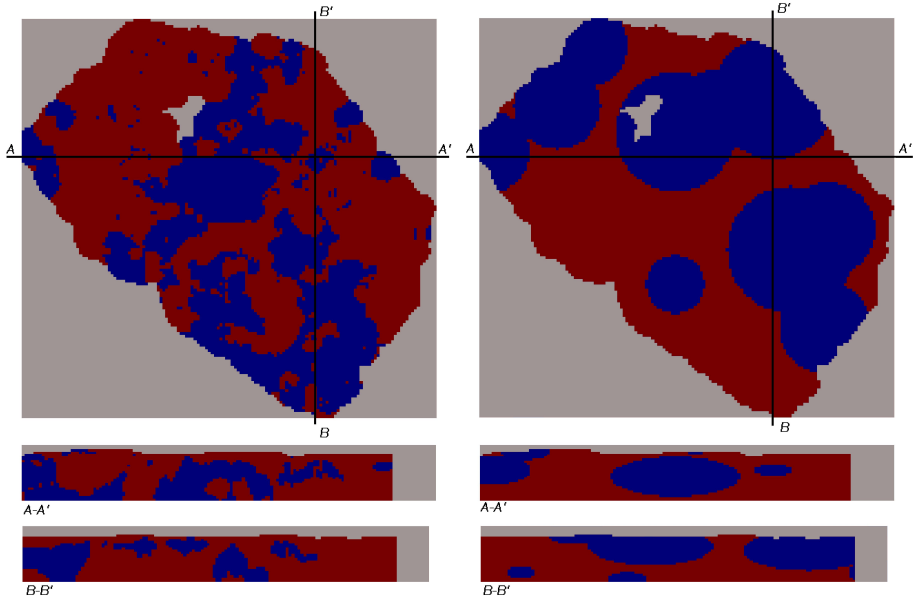

Fig. 5. Cross sections of TI1 (left) and TI2 (right). TI1 is converted from SkyTEM resistivity data while TI2 is generated by TiGenerator. Lateral cross section is taken at 10 m a.s.l., vertical exaggeration is 15. Red color indicates Quaternary sand and blue color Quaternary clay.

HESSD
10, 11829–11860, 2013

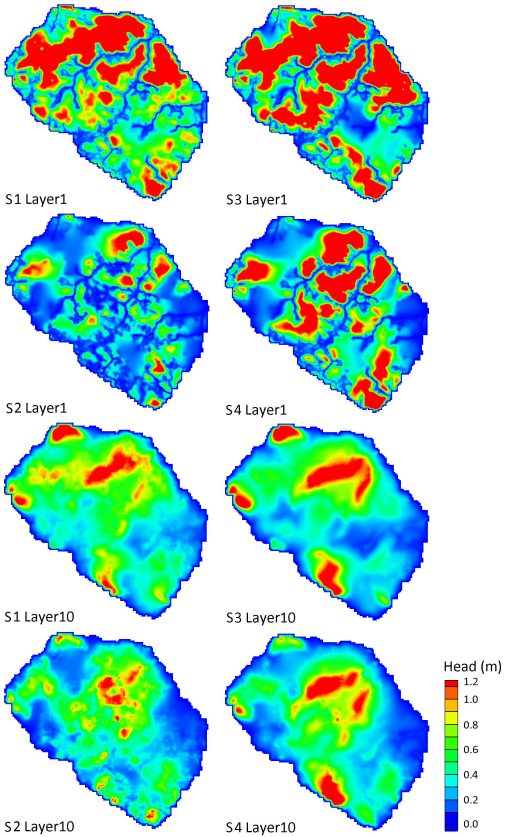

Fig. 6. Standard deviation of simulated hydraulic head from each scenario for layer 1 and layer 10.

HESSD
10, 11829–11860, 2013

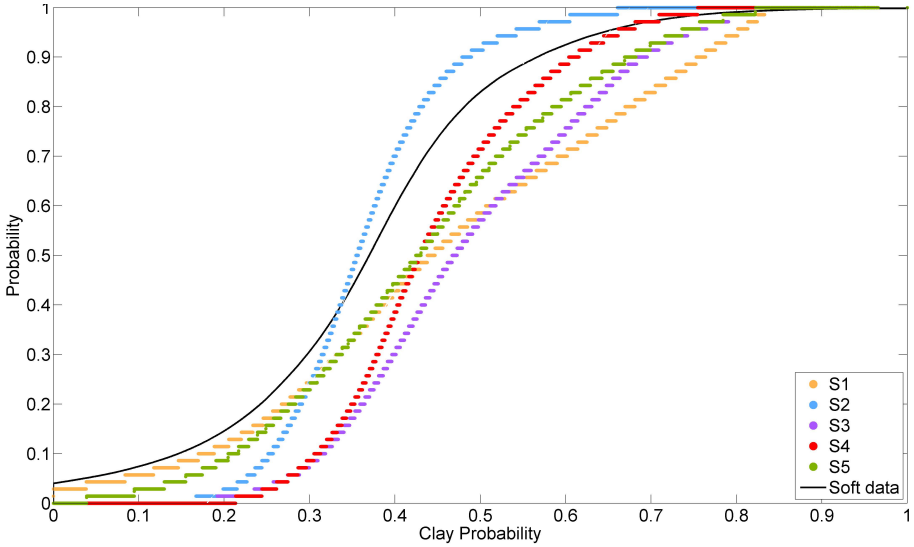

Fig. 7. Black line indicates cumulative probability distribution (CDF) of clay probability from soft data. Point plots are Q-Q plot of the average of realizations from each scenario against soft data.

HESSD
10, 11829–11860, 2013

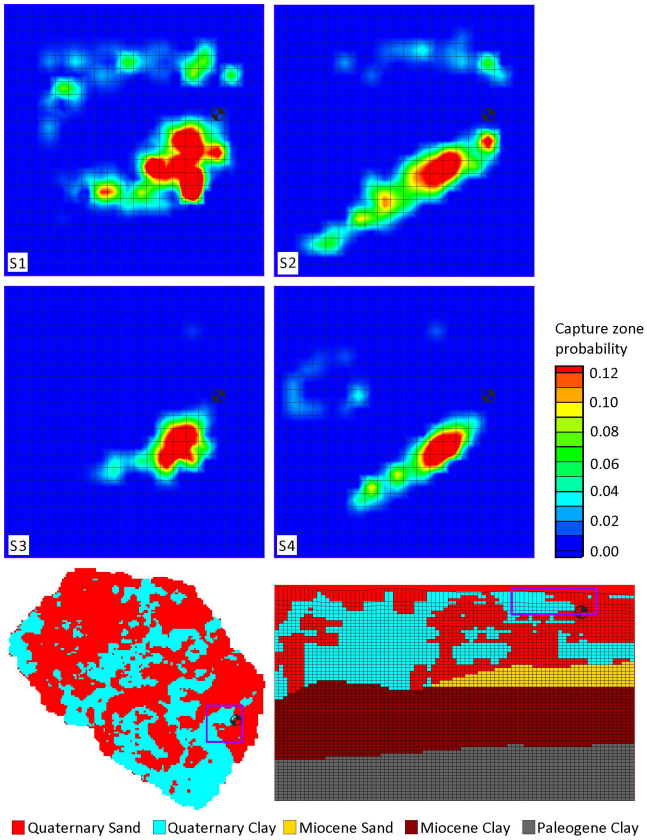

Fig. 8. The probabilistic capture zone of Well 1 from each scenario. Well location is illustrated in relation to the geological structure of the SSV model.

HESSD
10, 11829–11860, 2013

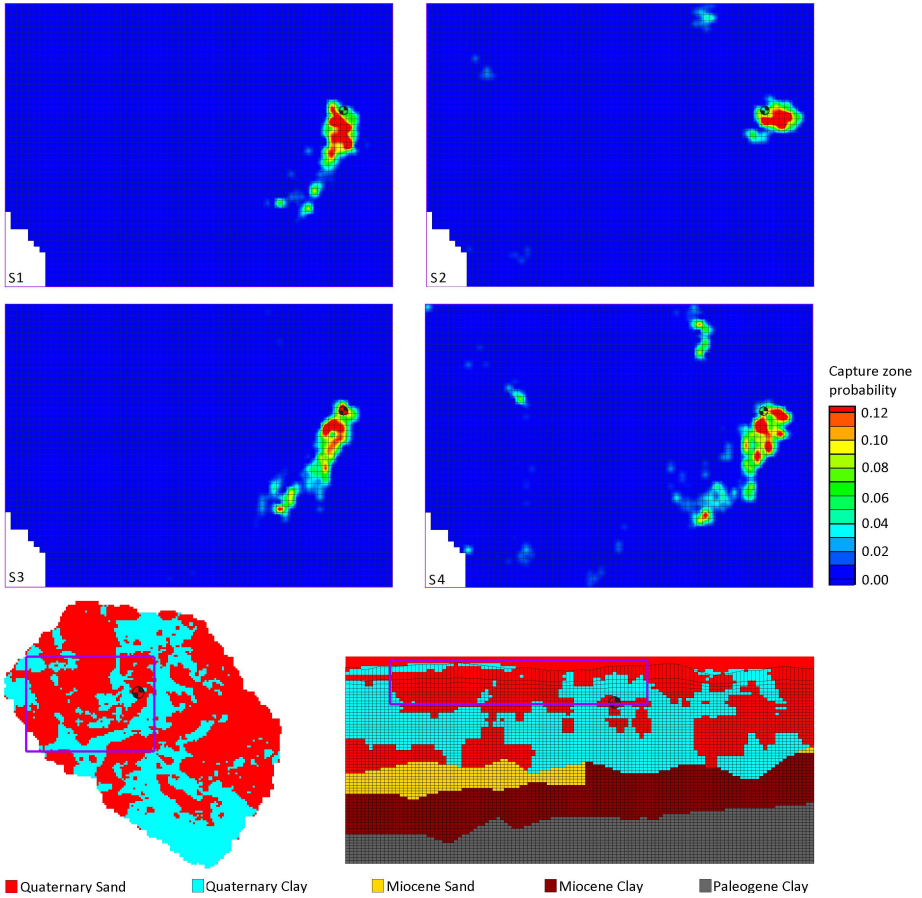

Fig. 9. The probabilistic capture zone of Well 2 from each scenario. Well location is illustrated in relation to the geological structure of the SSV model.

HESSD
10, 11829–11860, 2013

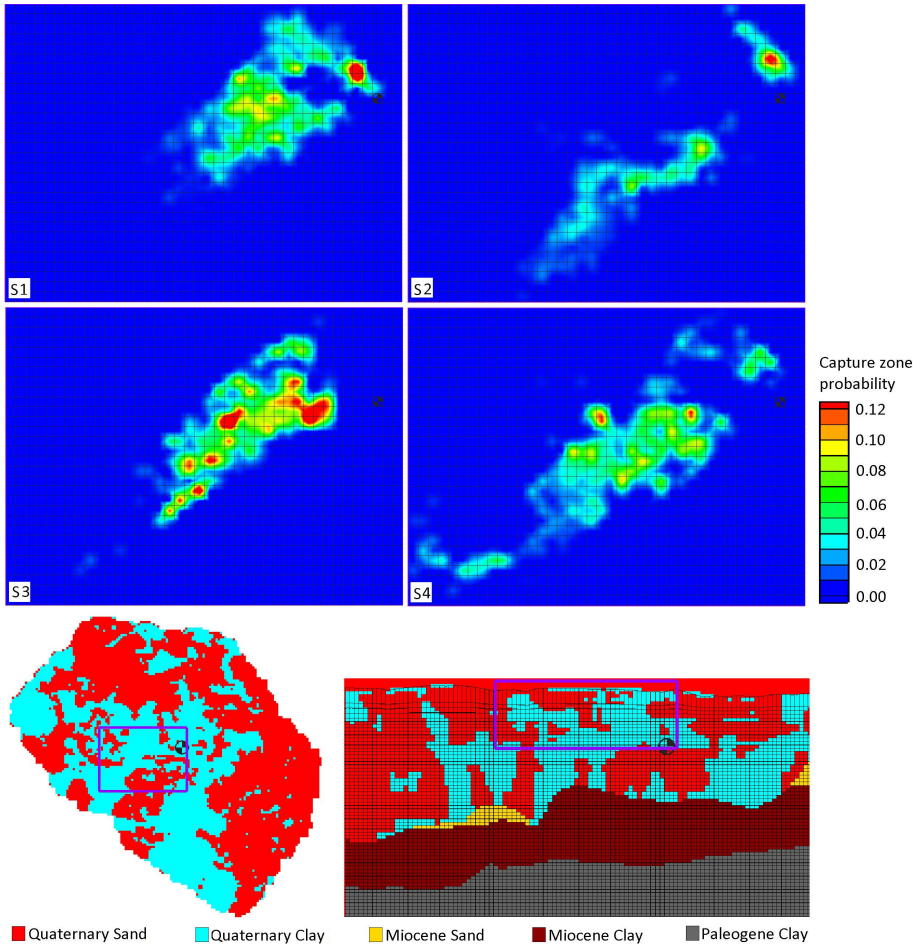

Fig. 10. The probabilistic capture zone of Well 3 from each scenario. Well location is illustrated in relation to the geological structure of the SSV model.

HESSD
10, 11829–11860, 2013